USGS Award Number GP15AP00090

Modeling injection-induced stress changes and potentially triggered seismicity in the south Kansas Mississippi Lime Play region

Elizabeth Hearn, Consulting Geophysicist
21 Valley Oak Street, Portola Valley CA 94028
Phone: (408) 334-8075
Fax: 650-329-5163
Email: hearn.liz@gmail.com

Grant Time Period: June 1, 2015 - May 31, 2016

Abstract

We have developed groundwater flow models to explore the possible relationship between wastewater injection and the November 2014 M 4.8 Milan, Kansas earthquake. In these models, we varied hydraulic properties of the Arbuckle Formation and the Milan earthquake fault zone, as well as the Milan earthquake hypocenter depth and fault zone geometry.

For a range of reasonable Arbuckle and fault zone hydraulic parameters, the modeled pore pressure increase at the Milan hypocenter exceeds a minimum (0.01 MPa) triggering threshold at the time of the earthquake. Critical factors include injection into the base of the Arbuckle Formation and the proximity of a conductive fault in the pre-Cambrian basement (i.e., a deep hypocenter for the east-dipping Milan fault). Given injection rates at nearby wells and likely hydrogeological properties for subsurface units and the fault zone, a pore pressure increase exceeding 0.1 MPa at the Milan hypocenter is unlikely to have occurred prior to the earthquake. This suggests that the Milan earthquake occurred on a critically stressed fault.

Introduction

During the past year, we (my contractor Chris Koltermann and I) have developed groundwater flow models to investigate pore pressure changes at the Milan earthquake hypocenter in response to wastewater injection at nearby, high-rate salt water disposal (SWD) wells. We upgraded these models throughout the grant period as new information from the study area became available. In this report, I describe (1) the hydrogeologic setting, based on our search of literature and Kansas government websites, (2) groundwater flow models developed during the grant period, and (3) results and implications of this work.

Hydrogeologic setting

<u>Hydrostratigraphy and aquifer properties.</u> In south-central Kansas, 5500-6000 feet (1700-1800 m) of Permian to Cambrian sediments overlie pre-Cambrian granite. These comprise thinly bedded shale, sandstone, limestone and dolomite layers, dipping less than ten degrees (Merriam, 1963). In Harper and Sumner counties, the top of the Ordovician Arbuckle Group occurs at depths between about 4400 to 4600 feet (1350-1400 m) below the ground surface. The formation is about 1000 feet (300 m) thick and consists mainly of coarsely granular, cherty dolomites. The dolomite at the top of the Arbuckle Group (the Cotter or Jefferson City Dolomite) is locally overprinted by karst features, owing to long-term subaerial exposure, because a major unconformity exists between this material and the layer above. Other karsted horizons exist within this formation wherever an unconformity is present. The top of the Arbuckle has been exploited for hydrocarbons (with peak production in the 1950's) and is now the principal target interval for brine injection in the area. Pre-Cambrian granite occurs below the Arbuckle, though only a few wells in the area penetrate this far.

The permeability of the Arbuckle Group may span several orders of magnitude. Carr et al. (1986) state that the average permeability, hydraulic conductivity, porosity and specific storage of the Arbuckle Group are 1.3×10^{-4} m^2, 0.15 m/d, 0.08 and 6.8×10^{-5} to 3.2×10^{-3}, respectively. More recent data from core sample tests and drill stem tests give a permeability range of 10^{-7} to 10^{-4} m/d, somewhat lower than the textbook range for carbonate rocks (Freeze and Cherry, 1979). However, measurements of k are scale dependent. Upscaled values of this parameter range from 10^{-5} to 10^{-3} m/d in the middle Arbuckle to 0.01-10 m/d in the more conductive upper and lower Arbuckle (Holubnyak et al., 2013). Karst overprinting and fractures may govern permeability in some areas, but lithofacies control of permeability (which is easier to represent in a large-scale model) is considered to be at least as important (Franseen et al., 2004).

Head elevations for all hydrostratigraphic units are inferred from contour plots from Carr et al. (1986). In the Arbuckle, flow is toward the east-southeast, with a gradient of approximately 0.0005. Pore fluid pressures in the Arbuckle Group are variable, but most fall below the hydrostatic pressure (hence, the formation is underpressured). In the 1980's, the piezometric surface elevation at Milan was reported to be 1100 to 1200 feet (335 to 366 m) above sea level, which is about 100 to 200 feet (30 to 60 m) below ground level (Carr et al., 1986). More recently, the piezometric surface for the Arbuckle Group at Wellington field was reported to be about 500 feet (150 m) below ground level (Watney, 2012). Pore pressures at the top and bottom of the Arbuckle were also reported to be 1.18×10^7 Pa and 1.47×10^7 Pa, respectively, at Wellington field (Scheffer, 2012). These pressures would indicate that the hydraulic head potentiometric surface is about 160 m below ground level at that location, and that there is no vertical gradient in hydraulic head (hence vertical flow) within the Arbuckle.

Wastewater injection wells. According to the March 2015 order by the Kansas Corporation Commission (Docket No. 15-CONS-770-CMSC; hereafter called the 2015 KCC order), five high-rate SWD wells were located within the model domain in 2014 (stars on Figure 1). Four of these wells were injecting wastewater at some point during 2013 and 2014. The well closest to the Milan hypocenter (Well D, aka "Dane", 4 km to the west) injects into the base of the Arbuckle formation while the other three active wells inject into the upper Arbuckle. Monthly injection rates at these wells ranged from 124,000 to 258,000 barrels per month (635 to 1325 m^3/day). During 2014, injection was under gravity feed at all of these wells but Well R ("Rizzo", 8 km west-southwest of the hypocenter), where maximum monthly injection pressure was 300 PSI (about 2 MPa). Monthly injection volumes at all four wells were represented in the model. Production and EOR wells, and wells injecting into shallower formations, were not represented.

The 2015 KCC order required that SWD well operators in Harper and Sumner Counties report monthly injection volumes. Since this was previously voluntary, the order resulted in an increase in data on injection volume and pressure data from Arbuckle SWD wells in the study area. Annual injection reports for 2015 were filed for twenty-four wells within the model domain (Tables 1a and 1b). Table 1a includes a well drilled in 2015 (Diana) as well as several that are just over 25 km from the Milan hypocenter; Table 1b excludes these wells. Of the 24 wells in Table 1b, four injected less than 30,000 BBL in 2015. Six of the wells are 20 to 25 km from the Milan hypocenter, and most of these are clustered at the southwest model boundary. The additional wells were added to the model mesh but were not "switched on" for this project, in which we focus on late 2014 (i.e., the time between increased injection rates and the Milan quake). We have found no 2014 injection volume data for several older wells located within 10 km of the Milan hypocenter (e.g., Birkholz, Robben and Hartman).

Fault zone and tectonic setting. Structural maps indicate that the Humboldt Fault Zone, a N-NE trending line of faults extends from the north into Oklahoma via eastern Sumner County. These steeply dipping faults, which fall along the Nemaha Anticline, cut pre-Cambrian and early Paleozoic rocks and show a maximum offset of about 100 feet (30 m; Merriam, 1963), and are still active (Steeples and Brosius, 1996). A dominantly right-lateral sense of slip has been inferred for these faults (McBee, 2003), though signs of reverse and normal faulting are also present. No other mapped faults are documented in Harper and Sumner counties or their immediate surroundings, though the dominant trends for mapped faults in Kansas are N-NE and NW-SE (Merriam, 1963). The Milan fault was identified because of the 2014 earthquake. Its geometry, defined by aftershocks and the mainshock focal mechanism (USGS NEIC, 2016), is consistent with the structures described above (i.e., N-NE striking, steeply dipping right-lateral fault).

Groundwater flow models

Model mesh. The model mesh (Figure 1) is approximately 40 km square, centered on the Milan earthquake epicenter, and aligned with one axis parallel to the N30E-striking Milan earthquake fault. It comprises 62 rows, 77 columns, and 23 layers. The fault core is modeled with two rows of 1 m-wide cells, and is within a 200 m-wide damage zone modeled with grid cells that increase in dimension outward from 1.5 m to 20 m. Outside the fault zone, model cell dimensions range from 20 m to 1 km. The left and right (i.e. NW and SE) sides of the model are constant head boundaries, set to enforce the regional flow gradient across the mesh and a hydraulic head of about 150 m below ground surface at the center of the model domain. The other sides and bottom are are no-flow boundaries. We have three versions of the mesh because of large uncertainties in the depth of the earthquake hypocenter. This is necessary because for a dipping fault, the depth of the hypocenter controls the proximity of the fault zone entry point (into the lower Arbuckle) to the SWD wells. The deeper the hypocenter, the closer the entry point to wells Dane and Rizzo (Figure 2).

Though one version of our model has made use of an unstructured mesh, we have gone with a structured grid (i.e. MODFLOW 2005; Harbaugh, 2005) in most of our calculations because (1) the smaller nodal spacing at the injection wells had little effect on modeled pore pressure change at the Milan hypocenter, and (2) plotting hydraulic head was less straightforward with the unstructured grid. Monthly injection volumes at the four high-rate SWD wells are from 2014 KCC records.

<u>*Parameter ranges and model suites.*</u> Hydraulic properties of the lower, middle and upper Arbuckle Formation and the fault damage zone were systematically varied, as well as the depth to the hypocenter (3, 5 or 7 km). Parameter ranges (Table 2) are based on published sources, as described in the previous section. Cases with low, medium and high values of hydraulic conductivity for each unit were forward modeled. The upper and lower Arbuckle were treated as anisotropic, with horizontal k component values twice the vertical component values (e.g. Freeze and Cherry, 1979). Crystalline bedrock and the middle Arbuckle were assumed to be isotropic. The storage coefficient S for aquifer units and the fault zone was 10^{-6}. S values of 10^{-7} and 10^{-5} were assumed for crystalline bedrock and the middle Arbuckle aquitard, respectively.

The Milan fault damage zone was modeled as anisotropic, with k along the damage zone ten times the value of k across the damage zone. The core was modeled as isotropic, with a lower k than that of the damage zone. One case with the Milan fault penetrating through the Arbuckle formation was also modeled (Model 6). The fault permeability architecture we assume, with a low-conductivity core embedded in a conductive damage zone, is based on several studies (e.g. Evans et al., 1997; Caine et al., 1996; Wibberley et al., 2008). The damage zone width we assume (200 m) is not varied. This width is consistent with seismic constraints on active faults (e.g., Li et al., 2000) and other induced seismicity models (Goebel et al., 2016), but falls at the high end of damage zone widths from field studies (e.g., Caine et al., 1996).

<u>*Model refinement during the work period.*</u> After the modeled mesh was developed and a suite of models sampling hydrogeologic parameters for the Arbuckle formation and the Milan fault zone were run, new information about the region became available. The following describes that information and how (or whether) we refined the model to account for it during the grant period.

Seismicity data from the USGS south Kansas network (Choy et al., 2016) constrains the hydraulic diffusivity of the Milan fault zone. Aftershocks along the Milan fault appear to have migrated to the edges of the rupture patch seven weeks to five months after the mainshock. Assuming that c (hydraulic diffusivity) $= r^2/(4\pi t)$ and a fault patch radius of about 1-2 km (Choy et al., 2016) one obtains c of 0.02 to 0.08 m^2/s. These values are consistent with other studies of seismicity migration along basement faults with induced earthquakes (in the 0.01 to 10 m^2/s range; El Hariri et al., 2010; Stabile et al., 2014; Hainzl et al., 2004). For our assumed specific storage $S = 10^{-6}$, this corresponds with k = 0.2 to 1.0 m/d, which is within the range we present (Table 2).

Seismic reflection profiles of the Arbuckle formation at the Wellington field show faults cutting the unit (Schwab et al., 2015). Faults can dramatically influence hydraulic head distributions by acting either as conduits or barriers to groundwater flow. Stable isotope and Br/Cl data indicate that the upper and lower Arbuckle aquifers are not hydraulically connected at Wellington field (Scheffer, 2012), so the faults are not efficient flow conduits in this area. After the 2015 AGU meeting (where the new Wellington field seismic profiles were presented), we added two models in which the Milan Fault cuts the Arbuckle Group (a variant of Model 1 is reported; Table 2). More models with the Arbuckle fault cutting the Arbuckle are underway.

As noted above, we identified several additional injection wells in the model region after March 2016 (when injection reports required by the 2015 KCC order were filed). These wells (Tables 1a and 1b) were added to the model mesh but were not “switched on” for this project. We have no data indicating rates of injection at any of the the newly identified wells within 10 km of the Milan hypocenter during 2014. However, 2015 injection reports show that these wells inject into the upper Arbuckle formation, and at a combined rate far lower rate than that of Well R, which is represented in the model (Table 1b).

Results and Discussion

Hydraulic properties of the lower, middle and upper Arbuckle Formation and the fault damage zone were varied, as well as the depth to the hypocenter. A reference model (Model 1) formed the basis for parameter exploration, and where hydraulic parameters in a particular unit were varied, others were held at the Model 1 values (Table 2) unless otherwise noted.

We find that a minimum triggering stress threshold of 0.01 MPa (Stein, 1999) is exceeded by the time of the Milan earthquake, for a range of aquifer parameters. Critical factors include injection into the base of the Arbuckle Formation and proximity of the entry point and hydraulic conductivity of the Milan fault (in the pre-Cambrian basement). The highest pore pressure change at the Milan hypocenter at the time of the earthquake (0.03 MPa) was obtained from a model with a conductive fault damage zone and lower Arbuckle (0.85 m/d and 0.25 to 2.5 m/d, respectively) and an assumed hypocenter depth of 7 km.

Sensitivity to model parameters. Figure 3 shows modeled pore pressures at the Milan hypocenter as a function of damage zone permeability and hypocenter depth. Pore pressures at the hypocenter were less sensitive to the hydraulic conductivity of the lower Arbuckle Group than to that of the damage zone, except for cases with a shallow assumed hypocenter. This is because most of the flow path is along the lower Arbuckle rather than the fault zone. The presence of a low-conductivity damage zone core is unimportant, likely because this core represents only a 2-m-wide portion of the 200-m-wide damage zone. A low-permeability fault core should play a more important role in models allowing the Arbuckle fault to penetrate the Arbuckle Group.

For the default (moderate) hydraulic conductivity case, allowing the Milan fault to penetrate the Arbuckle Group has little effect on inferred pore pressure change at the Milan hypocenter. Figure 4 shows that when the fault cuts the Arbuckle, modeled pore pressures at the Milan hypocenter decrease slightly, indicating a reversed hydraulic gradient (upward flow) exists across the middle Arbuckle, and that elevated pore pressures in the lower Arbuckle are being communicated upward into the upper Arbuckle. Figure 4 also shows models with varied conductivity in the upper Arbuckle aquifer. For a more conductive upper Arbuckle, the modeled pore pressure at the Milan hypocenter is lower. This again suggests upward flow through the middle Arbuckle: for a lower value of k, heads in the upper Arbuckle are greater (due to injection from well R and others), reducing the magnitude of the head gradient between this unit and the overpressured lower Arbuckle. This reversed hydraulic gradient is sensitive to the assumed initial pore pressures in the Arbuckle Group, which are poorly constrained in the model region. It is also sensitive to hydraulic parameters of the middle Arbuckle and the fault zone. Stable isotope data indicate that the upper and lower Arbuckle aquifers are not hydraulically connected in the model region (Scheffer, 2012), suggesting that the fault is not an effective conduit connecting the upper and lower Arbuckle aquifers.

Implications and targets for future research. If the Milan earthquake hypocenter depth is consistent with aftershocks (4 to 7 km; Choy et al., 2016), a conductive fault zone is required for pore pressures to exceed the triggering threshold. For our models with a 200-m-wide damage zone, models with k = 0.85 were required; higher k values would be required for narrower damage zones. Given the fault orientation and the E-W orientation of the maximum horizontal stress (Zoback, 1992), the Milan earthquake fault is likely to have been critically stressed, consistent with its high hydraulic conductivity (Barton et al., 1995; Evans et al., 1997). A low Coulomb stress increase at the hypocenter is consistent with other induced earthquakes in the central U.S. (e.g., Hornbach et al., 2015; Keranen et al., 2014; Yeck et al., 2016). As the pore pressure front migrates further from high-rate wells, additional critically-stressed fault zones may be triggered.

Given injection rates and likely hydrogeological properties for subsurface units and the fault zone, a pore pressure increase exceeding a tenth of a MPa at the Milan hypocenter is unlikely to have occurred before the earthquake. Simply put, there is only so much water being injected and it is difficult to make this volume cause large increases in pore pressure at the hypocenter. We are constrained by the rapid onset of seismicity in response to increased injection rates to have a fairly high value of hydraulic diffusivity (c) for the fault damage zone and lower Arbuckle. Our assumed S in the aquifers and shear zone (10^{-6}) is already on the low end of an admissible range for confined aquifers. To obtain higher pore pressures at the hypocenter while reproducing the rapid onset of seismicity, we can model lower values of both S and k. This would move S below reasonable ranges for confined aquifers (e.g. Freeze and Cherry, 1979). Other parameters to explore include the width of the damage zone and the degree of anisotropy of aquifers and the fault damage zone.

The large injection volumes into the upper Arbuckle do not appear to have caused notable pore pressure changes at the Milan hypocenter by the time of the November 2014 earthquake. However, this may change if local seismicity has altered the permeability of faults that cut the Arbuckle. Though stable isotope data indicate that the upper and lower Arbuckle aquifers are not hydraulically connected at Wellington Field (in the model region, about 15 km east of the Milan hypocenter; Scheffer, 2012), they do indicate hydraulic connection at Cutter Field, about 250 km to the west (Watney et al., 2015). If pore pressure changes from the upper Arbuckle are eventually communicated to the lower Arbuckle (and hence to faults in the bedrock below), hazard levels in the region could remain elevated in southern Kansas for some time, even for reduced rates of wastewater injection. Tracer tests, geochemical analyses of water from the upper and lower Arbuckle, and detailed measurements of pore pressures in both Arbuckle aquifers could provide insight on whether their degree of hydraulic connection has changed. This information would be a great help in modeling pore pressure evolution and managing seismic hazard in the region.

References

Barton, C. A., M. D. Zoback and D. Moos (1995), Fluid flow along potentially active faults in crystalline rock, Geology, 23(8), 683-686.

Caine, J. S., J. P. Evans and C. B. Forster (1996), Fault zone architecture and permeability structure, Geology, 24(11), 1025-1028.

Carr, J. E. et al. (1986), Geohydrology of and potential for fluid disposal in the Arbuckle aquifer in Kansas, Open File Report 86-491, US Geological Survey.

Choy, G. L., J. L. Rubinstein, W. L. Yeck, D. E. McNamara, C. S. Mueller and O. S. Boyd (2016), A Rare Moderate−Sized (Mw 4.9) Earthquake in Kansas: Rupture Process of the Milan, Kansas, Earthquake of 12 November 2014 and Its Relationship to Fluid Injection, Seis. Res. Lett., DOI: 10.1785/0220160100, 14 September 2016.

El Hariri, M., R. E. Abercrombie, C. A. Rowe and A. F. Do Nascimento (2010), The role of fluids in triggering earthquakes: observations from reservoir induced seismicity in Brazil, Geophysical J. Int., 181(3), 1566-1574.

Evans, J. P., C. B. Forster and J. V. Goddard (1997), Permeability of fault-related rocks, and implications for hydraulic structure of fault zones, J. Struct. Geol., 19(11), 1393-1404.

Franseen, E. K., A. P. Byrnes, J. R. Cansler and T. Carr (2004), The Geology of Kansas: Arbuckle Group, Kansas Geological Survey.

Freeze, R. A. and J. A. Cherry (1979), Groundwater, Prentice-Hall, ISBN-10:0133653129.

Goebel, T. H. W., S. M. Hosseini, F. Cappa, E. Hauksson, J. P. Ampuero, F. Aminzadeh and J. B. Saleeby (2016), Wastewater disposal and earthquake swarm activity at the southern end of the Central Valley, California, Geophys. Res. Lett., DOI 10.1002/2015GL066948.

Hainzl, S. (2004), Seismicity patterns of earthquake swarms due to fluid intrusion and stress triggering. Geophys. J. Int., 159(3), 1090-1096.

Harbaugh, A.W. (2005), MODFLOW-2005, the U.S. Geological Survey modular ground-water model -- the Ground-Water Flow Process, U.S. Geological Survey Techniques and Methods 6-A16.

Holubnyak, Y., W. L. Watney, J. Rush, T. R. Birdie, M. Fazelalavi and J. Raney (2013), Dynamic Simulation of Pilot Scale CO2 Injection in the Arbuckle Saline Aquifer at Wellington Field in Southern Kansas, AGU Fall Meeting Abstract H21L-04.

Hornbach, M. J., H. R. DeShon, W. L. Ellsworth, B. W. Stump, C. Hayward, C. Frohlich, H. R. Oldham, J. E. Olson, M. B. Magnani, C. Brokaw and J. H. Luetgert (2015), Causal factors for seismicity near Azle, Texas, Nature Communications, 6, doi:10.1038/ncomms7728.

Keranen, K. M. et al. (2014), Sharp increase in central Oklahoma seismicity since 2008 induced by massive wastewater injection, Science, 345, 448-451.

Koltermann, C. and E. Hearn (2015), Numerical Models of Pore Pressure and Stress Changes along Basement Faults due to Wastewater Injection: Applications to Potentially Induced Seismicity in Southern Kansas, Abstract S13B-2823, 2015 AGU Fall Meeting.

Li, Y.-G., J. E. Vidale, K. Aki, and F. Xu (2000), Depth-dependent structure of the Landers fault zone from trapped waves generated by aftershocks, J. Geophys. Res., 105(B3), 6237–6254, doi: 10.1029/1999JB900449.

McBee, W. (2003), The Nemaha and other strike-slip faults in the Midcontinent U.S.A., AAPG Mid-continent section meeting, October 13, 2003, AAPG Search and Discovery Article #10055.

Merriam, D. E. (1963), The Geologic History of Kansas, Kansas Geological Survey Bull. 162.

Parotidis M., Rothert E., Shapiro S.A., 2003. Pore-pressure diffusion: a possible triggering mechanism for the earthquake swarms 2000 in Vogtland/NW-Bohemia, central Europe, Geophys. Res. Lett., 30, 20, doi. 10.1029/2003GL018110.

Scheffer, A. (2012), Geochemical and Microbiological Characterization of the Arbuckle Saline Aquifer, a Potential CO_2 Storage Reservoir; Implications for Hydraulic Separation and Caprock Integrity, University of Kansas Master's Thesis.

Schwab, D., T. Bigdoli and M. H. Taylor (2015), Characterizing the potential for fault reactivation related to CO2 injection through subsurface structural mapping and stress field analysis, Wellington Field, Sumner County, KS, AGU Fall Meeting Abstract S13B-2822.

Shapiro S.A., E. Huenges and G. Borm (1997), Estimating the crust permeability from fluid-injection-induced seismic emission at the KTB site, Geophys. J. Int., 131, F15–F18.

Stabile, T. A., A. Giocoli, V. Lapenna, A. Perrone, S. Piscitelli, S. and L. Telesca (2014), Evidence of Low−Magnitude Continued Reservoir−Induced Seismicity Associated with the Pertusillo Artificial Lake (Southern Italy), Bull. Seis. Soc. Am., 104, doi: 10.1785/0120130333.

Stabile, T. A., A. Giocoli, A. Perrone, S. Piscitelli and V. Lapenna (2014), Fluid injection induced seismicity reveals a NE dipping fault in the southeastern sector of the High Agri Valley (southern Italy), Geophys. Res. Lett., 41(16), 5847-5854.

Steeples, D. W. and L. Brosius (1996), Earthquakes, Kansas Geological Survey Public Information Circular 3, June 1996 (revised July 2014), http://www.kgs.ku.edu/Publications/pic3/PIC3_2014_revision.pdf (accessed May 22, 2016).

Stein, R. S. (1999), The role of stress transfer in earthquake occurrence, Nature, 402, 605-609.

USGS NEIC (2016) Moment tensor: http://earthquake.usgs.gov/earthquakes/eventpage/usc000swru#moment-tensor, accessed 30 September 2016. Origin: http://earthquake.usgs.gov/earthquakes/eventpage/usc000swru#origin accessed 30 September 2016.

Walder, J. S. (1984), Coupling between fluid flow and deformation in porous crustal rocks, Doctoral dissertation, Stanford University Department of Geophysics.

Walsh, F. R. and M. D. Zoback (2015), Oklahoma's recent earthquakes and saltwater disposal, Sci. Adv., 1, e1500195.

Wang, H. (2000), Theory of Linear Poroelasticity with Applications to Geomechanics and Hydrogeology, Princeton University Press, ISBN: 9780691037462.

Watney, M. L. (2012), presentation for U.S. Department of Energy National Energy Technology Laboratory Carbon Storage R&D Project Review Meeting, Developing the Technologies and Building the Infrastructure for CO2 Storage, 8/21/12, http://www.kgs.ku.edu/PRS/Ozark/SmallScale/2012/Watney_DE-FE0006821__FY12_Carbon_Storage_Review_8-27-12.pdf.

Watney, W. L., et al. (2014), Geologic Carbon Storage in the Lower Ordovician Arbuckle Group Saline Aquifer in Kansas", 2014 NGWA Groundwater Summit.

Watney, M. L. et al. (2015), Modeling CO_2 Sequestration in Saline Aquifer and Depleted Oil Reservoir to Evaluate Regional CO_2 Sequestration Potential of Ozark Plateau Aquifer System, South-Central Kansas, Wrap Up Presentation, DOE-NETL, Pittsburgh PA Feb. 12, 2015.

Watney, M. L. et al. (2016), Geologic Carbon Sequestration Research in Kansas: Subsurface Storage Capacities and Pilot Tests for Safe and Effective Disposal, Kansas NextStep Oil and Gas Seminar, Hays, Kansas, April 5-7, 2016.

Wibberley, C. A. et al. (2008), Recent advances in the understanding of fault zone internal structure: a review, in Wibberley, C. A. et al., eds.,The Internal Structure of Fault Zones: Implications for Mechanical and Fluid-Flow Properties, 299, 5–33, Geol. Soc. London.

Yeck, W. L., M. Weingarten, H. M. Benz, D. E. McNamara, E. A. Bergman, R. B. Herrmann, J. L. Rubinstein, and P. S. Earle (2016), Far-field pressurization likely caused one of the largest injection induced earthquakes by reactivating a large preexisting basement fault structure, Geophys. Res. Lett., 43, 10,198–10,207, doi:10.1002/2016GL070861.

Zhang, Y. et al. (2013), Hydrogeologic controls on induced seismicity in crystalline basement rocks due to fluid injection into basal reservoirs, Groundwater, 51(4), 525-538.

Zoback, M.L. (1992), First and second-order patterns of stress in the lithosphere: The World Stress Map Project, J. Geophys. Res., 97, 11703-11728.

Publications from Work Performed under this Award

Hearn, E. H., C. Koltermann and J. Rubenstein (2016), Numerical Models of Pore Pressure and Stress Changes along Basement Faults due to Wastewater Injection: Applications to Potentially Induced Seismicity in Southern Kansas, in preparation for BSSA.

Koltermann, C. and E. Hearn (2015), Numerical Models of Pore Pressure and Stress Changes along Basement Faults due to Wastewater Injection: Applications to Potentially Induced Seismicity in Southern Kansas, Abstract S13B-2823, 2015 AGU Fall Meeting.

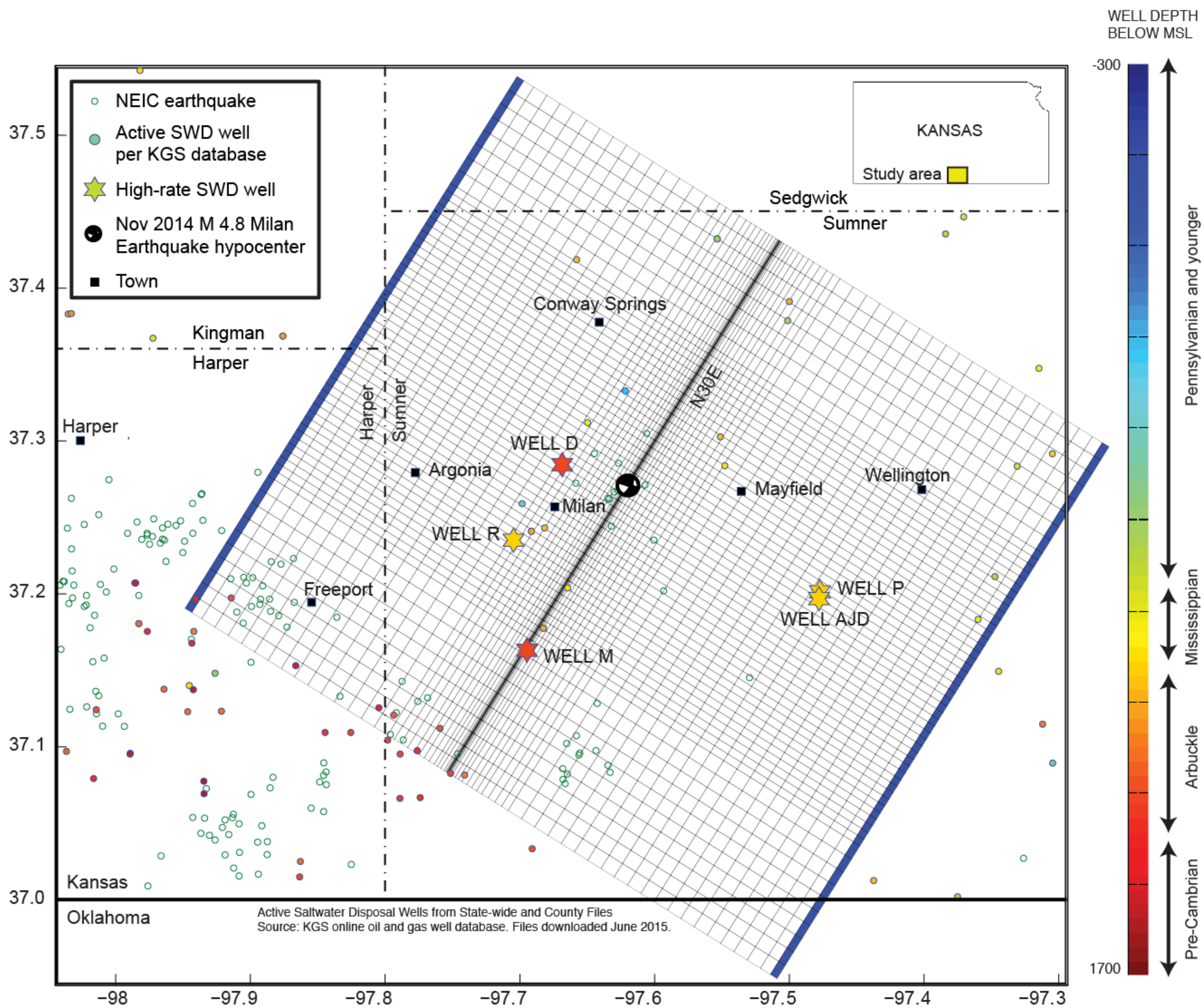

Figure 1. Plan view of MODFLOW model mesh, showing locations of modeled SWD wells (colored stars) and other SWD wells in the region (colored circles). Well symbol colors are keyed to completion depth. Open circles show earthquakes through mid-2015.

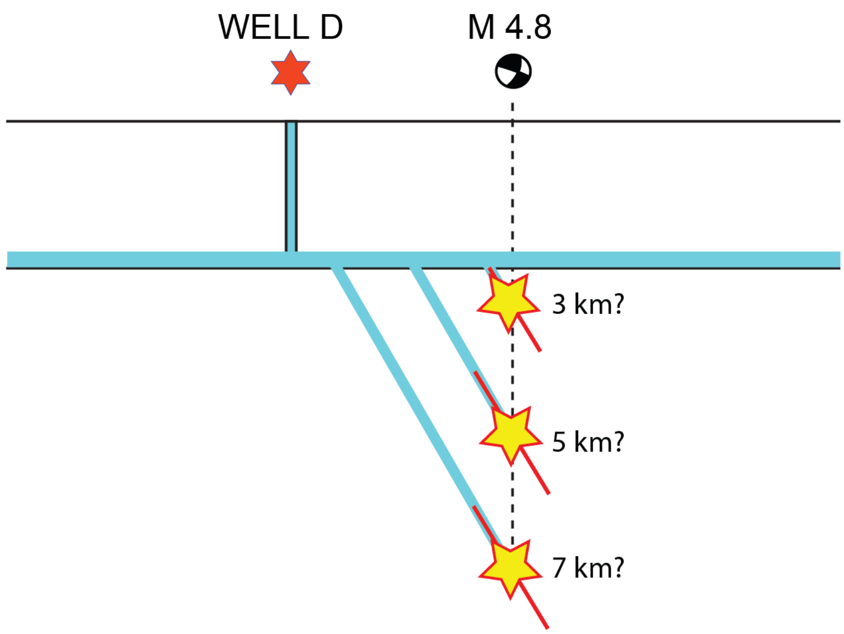

Figure 2. Cartoon profile view showing east-dipping Milan fault rupture plane given hypocenters at different assumed depths. The entry point from the lower Arbuckle to the transmissive fault zone depends on hypocenter depth. For greater hypocenter depths, proportionally more of the travel path for the pore pressure front is in the fault zone (rather than the lower Arbuckle) and the entry point is closer to Well D.

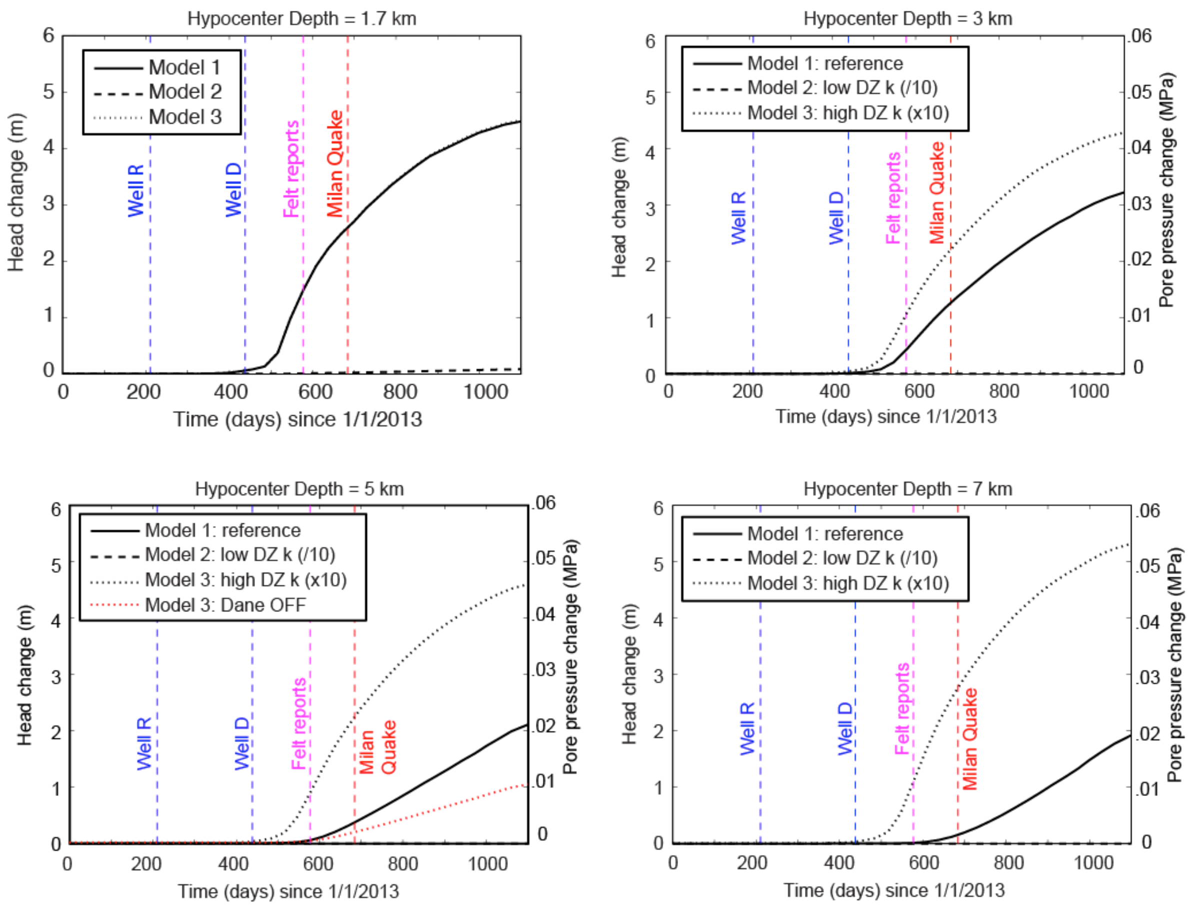

Figure 3. Modeled pore pressure as a function of time for three instances of fault zone conductivity. Each panel represents a different hypocenter depth. For the shallowest assumed hypocenter depth, shear zone conductivity is less important because nearly the entire travel path is along the conductive lower Arbuckle. At greater hypocenter depths, proportionally more flow is along the fault zone, and its hydraulic properties become more important. For the most likely hypocenter depths (5-7 km), Model 3 (incorporating the most conductive damage zone) suggests pore pressure changes exceeding 0.02 MPa at the Milan hypocenter at the time of the earthquake, consistent with Coulomb stress changes exceeding 0.014 MPa (for a friction coefficient of 0.7). For beyond 2015, the mean 2014 injection rates at each well were assumed.

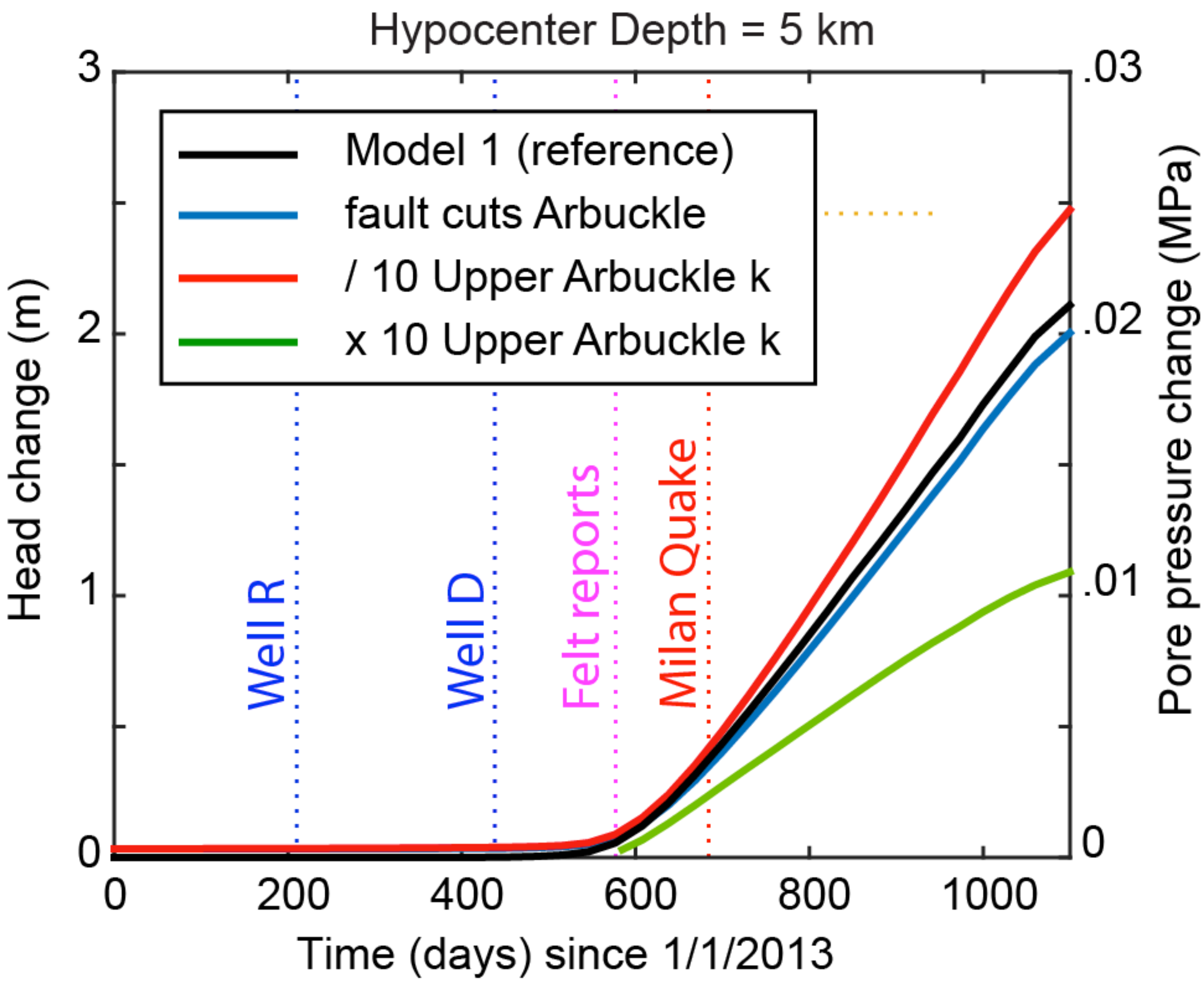

Figure 4. Modeled pore fluid pressure at the Milan earthquake hypocenter as a function of time. Sensitivity to upper Arbuckle hydraulic conductivity (k) suggests a reverse hydraulic gradient, resulting in increased pore pressures at the Milan hypocenter as the upper Arbuckle k is reduced. When the Milan fault is modeled crossing the Arbuckle, the pore fluid pressure drops very slightly, consistent with this finding. This conclusion is sensitive to assumed pore pressures in the upper and lower Arbuckle at the start of our model period (January, 2013), as well as hydraulic properties of the fault zone and the middle Arbuckle aquitard.

SWD WELL ID	API #	LAT	LON	ELEV FT (M)	DEPTH FT (M)	Plug Back Total Depth FT (M)	DATE COMPLETED	INJECTION FORMATION	PACKER DEPTH FT (M)	Arbuckle Top FT (M)	Notes
WELL D Dane	15-191-22726-0000	37.284492	-97.668505	1240 (378)	5505 (1678)		April 2014	All Arbuckle	4616 (1407)	4527 (1380), 4486 (1367)	4527 ft (geol log) 4486 ft (electric log) in well Hausaman 1 nearby (15-191-00433)
WELL R Rizzo	15-191-22682-0001	37.2350582	-97.7046419	1215 (370)	4589 (1399)		June 2013	Upper Arbuckle	4581 (1396)	4460 (1359)	
WELL A AJDowis	15-191-01384-0002	37.1915697	-97.4863475	1225 (373)	4482 (1367)		Mar 2013	Simpson, Upper Arbuckle	4160 (1268)	4241* (1293*)	*Simpson top - no data on Arbuckle top
WELL P Perth	15-191-22699-0001	37.2015256	-97.4763279	1244 (379)	4800 (1463)		July 2014	Upper to middle Arbuckle	4377 (1334)	4368 (1331)	
WELL M Madison	15-191-22686-0000	37.1626032	-97.6936169	1259 (384)	5296 (1615)		Aug 2013	All Arbuckle	4783 (1458)	4663 (1421)	
WELL H Hartman	15-191-21267-0000	37.2409800	-97.6914000	1206 (368)	4732 (1442)		May 1981	Upper Arbuckle	no record	4456 (1358)	
WELL B Birkholz	15-191-00449-0001	37.2264700	-97.7186400	1218 (371)	4606 (1404)		Sept 1969	Upper Arbuckle	no record	4433 (1351)	
WELL R Robben	15-191-20869-0000	37.2430883	-97.6815259	1182 (360)	4663 (1421)		April 1979	Upper Arbuckle	no record	4438 (1353)	"4453-4663 ft open hole" (1357m-1421m)
Love OWWO 3	15-191-30404-0002	37.26905	-97.69793	1249 (380)	4364 (1330)		Dec 1974	Simpson and shallower	3001 (914.7)	4361* (1329)	*Simpson top - no data on Arbuckle top
Duke 3404	15-191-22729-0000	37.0974075	-97.7760340	1257 (383)	5728 (1746)		June 2014	All Arbuckle			
Misak 2	15-191-21738-0000	37.1206409	-97.7936342	1252 (382)	5300 (1615)		Nov 1984	All Arbuckle	4814 (1467)	4928 (1502)	"open hole Arbuckle 4928-5305 ft" (1502-1617 m)
Muhlenbruch	15-191-20671-0001	37.20384	-97.66441	1218 (371)	4424 (1348)		July 1977	Upper Arbuckle			
Small 2	15-191-00050-0001	37.1775133	-97.6824377	1263 (385)	4850 (1478)		Dec 1978	Simpson + Upper Arbuckle	4572 (1394)	4614 (1406)	ltd = logged total depth = 4837 ft (1474 m)
Latimer	15-191-19069-0000	37.1948100	-97.4771900	1228 (374)	4422 (1348)		Feb 1946	Upper Arbuckle			
Ivie-1	15-191-20224-0000	37.3025800	-97.5511000	1318 (402)	4725 (1440)		Aug 1970	Upper Arbuckle		4436 (1352)	cemented casing to 4439 ft (1353 m)
Metzen-1	15-191-20522-0000	37.2838200	-97.5477900	1281 (390)	4572 (1394)		June 1975	Upper Arbuckle		4364 (1330)	casing set and cemented to 4466 ft (1361 m)
Orr	15-191-10151-0001	37.3590000	-97.6734100	1382 (421)	4780 (1457)		Feb 1958	Upper Arbuckle			
HEG Whitten	15-191-22502-0000	37.1959200	-97.4876200	1238 (377)	5368 (1636)		June 2007	All Arbuckle		4353 (1327) kb	casing cemented in (?) to 4403 ft (1342 m). Plugged back to 4290 and converted to oil well (screened in the Simpson formation) in 2013. (API # -0001)
Forrest	15-191-22730-0000	37.1043296	-97.7980438	1266 (386)	5490 (1673)		May 2014	All Arbuckle			1974 oil well 15-191-20424 800 ft away: Simpson top is 4793 ft (1461 m)
Diana	15-077-21988-0001	37.1254944	-97.8046142	1265 (386)	6017 (1834)	5689 (1734)	June 2015	All Arbuckle	5094 (1553)	4930 (1503)	5094 ft (1553 m) = depth of shoe, casing ends at 5095 ft, open hole to 5689 ft (1734 m). Granite at 5992 ft (1826 m).
Gaylord	15-191-22717-0000	37.1120553	-97.7591950	1233 (376)	5416 (1651)		April 2014	All Arbuckle			
Frantz	15-191-01547-0002	37.3603806	-97.6637527	1367 (417)	4774 (1455)		July 1960	Upper Arbuckle		4418 (1347)	4350 (1326 m) = top of Simpson, casing cemented to 4506 (1373 m)
Murphy	15-191-22733-0000	37.0952715	-97.7888482	1254 (382)	5556 (1694)		May 2014	Upper and Middle Arbuckle			
Love 1	15-191-43059-0002	37.4522700	-97.5452600	1322 (403)	4304 (1312)		1927	Upper Arbuckle		4214 (1285)	date of conversion to SWD well from oil well not recorded
Mies 2	15-191-20302-0000	37.4185100	-97.6578300	1331(406)	4747 (1447)		October 1971	Simpson		4265* (1300)	*Simpson top
Renner 4a	15-191-22754	37.3911270	-97.4998920	1328 (405)	4850 (1479)		July 2014	Upper Arbuckle	4460 (1360)	4300 (1311)	open hole 4475-4850; Arbuckle top is from 1956 D and A well 15-191-01487, 100 ft north
Teague-Brooner	15-191-00542-0002	37.3694341	-97.4379340	1303 (397)	4323 (1318)		April 2014	Upper Arbuckle			
Kingston	15-191-22736-0000	37.0825469	-97.7514665	1244 (379)	5557 (1694)		June 2014	Upper to Middle Arbuckle		4986 (1520)	Arbuckle top estimated from abandoned 1962 well 15-191-00765 one mile to the east
Blitzberg	15-191-22721-0000	37.0662776	-97.7889229	1230 (375)	5622 (1714)		Jan 2014	Upper to Middle Arbuckle			Could not make sense of logs from two adjacent wells (chert to 9100 feet? No Arbuckle?)
Junebug	15-191-22681-0001	37.0687908	-97.7671408	1241 (378)	5533 (1687)		July 2013	Upper to Middle Arbuckle	5122 (1562)	5085 (1550)	open hole below packer/casing
Windsor	15-191-22739	37.0668161	-97.7739533	1242 (379)	5590 (1704)		June 2014	Upper to Middle Arbuckle		5085 (1550)	assume same Arbuckle top as Junebug 15-191-22681, 1 mi to the E-NE
Ritter	15-191-22722-0000	37.0814663	-97.7408430	1242 (379)	5155 (1572)		April 2014	Upper Arbuckle		4984 (1520)	Arbuckle top estimated from abandoned 1962 well 15-191-00765 600 ft to the NE

Table 1a. SWD wells injecting into the Arbuckle Group, within the model region. Most of these wells were identified during the spring of 2016, when operators filed injection reports as mandated by the March 2015 order by the Kansas Corporation Commission (Docket No. 15-CONS-770-CMSC).

	WELL ID	LAT	LON	Model E coord (km)	Model N coord (km)	E dist to HC (km)	N dist to HC (km)	total dist to M 4.8 epicenter (km)	2015 volume
WELL D Dane	15-191-22726-0000	37.284492	-97.668505	29.5197	32.8618	-4.38130	-0.80040	4.45	263592.00
WELL R Rizzo	15-191-22682-0001	37.2350582	-97.7046419	29.5	26.5145	-4.40100	-7.14770	8.39	2842674.00
WELL A AJDowis	15-191-01384-0002	37.1915697	-97.4863475	48.6057	31.9716	14.70470	-1.69060	14.80	nr (1209600 in 2014)
WELL P Perth	15-191-22699-0001	37.2015256	-97.4763279	48.8193	33.371	14.91830	-0.29120	14.92	1494949.00
WELL M Madison	15-191-22686-0000	37.1626032	-97.6936169	34.3643	20.0365	0.46330	-13.62570	13.63	0.00
WELL H Hartman	15-191-21267-0000	37.24098	-97.6914	30.1839	27.668	-3.71710	-5.99420	7.05	347395.00
WELL B Birkholz	15-191-00449-0001	37.22647	-97.71864	28.9063	25.071	-4.99470	-8.59120	9.94	114672.00
WELL R Robben	15-191-20869-0000	37.2430883	-97.6815259	30.8218	28.3071	-3.07920	-5.35510	6.18	109500.00
Latimer 2	15-191-19069-0000	37.19481	-97.47719	49.1261	32.6874	15.22510	-0.97480	15.26	19039.00
Small 2	15-191-00050-0001	37.1775133	-97.6824377	34.3196	21.9633	0.41860	-11.69890	11.71	25930.00
Gaylord	15-191-22717-0000	37.1120553	-97.759195	32.1552	12.2823	-1.74580	-21.37990	21.45	209449.00
Love 3 OWWO	15-191-30404-0002	37.26905	-97.69793	28.1267	30.0783	-5.77430	-3.58390	6.80	90000.00
Orr	15-191-10151-0001	37.359	-97.67341	25.0094	39.8074	-8.89160	6.14520	10.81	77975.00
Jordan Sailor	15-191-22481-0000	37.3119329	-97.6497178	29.4333	36.329	-4.46770	2.66680	5.20	71424.00
Muhlenbruch	15-191-20671-0001	37.20384	-97.66441	34.3112	25.286	0.41020	-8.37620	8.39	981.00
Duke 3404	15-191-22729-0000	37.0974075	-97.776034	31.6808	10.1311	-2.22020	-23.53110	23.64	334932.00
Misak2	15-191-21738-0000	37.1206409	-97.7936342	29.0453	11.5871	-4.85570	-22.07510	22.60	79935.00
Ivie 1	15-191-20224-0000	37.30258	-97.5511	37.4933	39.7839	3.59230	6.12170	7.10	38475.00
Metzen 1	15-191-20522-0000	37.28382	-97.54779	38.7876	38.1267	4.88660	4.46450	6.62	68985.00
Whitten	15-191-22502-0000	37.19592	-97.48762	48.267	32.3336	14.36600	-1.32860	14.43	nr
Forrest	15-191-22730-0000	37.1043296	-97.7980438	29.6133	9.8245	-4.28770	-23.83770	24.22	1247605.00
Diana	15-077-21988-0001	37.1254944	-97.8046142	27.9363	11.5689	-5.96470	-22.09330	22.88	1535539.00
Frantz	15-191-01547-0002	37.3603806	-97.6637527	25.6712	40.3665	-8.22980	6.70430	10.61	163084.00
Murphy	15-191-22733-0000	37.0952715	-97.7888482	30.8192	9.3598	-3.08180	-24.30240	24.50	356421.00

Table 1b. SWD wells injecting into the Arbuckle Group, within 25 km of the hypocenter. Distances to the Milan hypocenter and 2015 injection volumes are shown. Wells shown in blue are over 20 km from the Milan hypocenter. Wells shown in green are within the model domain but injected at a low rate in 2015. The top five wells on this list were included in the models described in this report; additional wells in black were added subsequently.

ID	Description	Lower Arbuckle K (m/d)	Middle Arbuckle K (m/d)	Upper Arbuckle K (m/d)	Fault damage zone K (m/d)	Fault core K (m/d)	Fault cuts Arbuckle?	Assumed HC depth (km)
Model 1	Reference model	Kx=Ky=0.25 Kz=0.12	Kx=Ky=Kz=8.0E-04	Kx=Ky=0.25 Kz=0.12	8.5E-03 across, 8.5E-02 along	8.0E-04	No	5
Model 2	Low-permeability shear zone	Kx=Ky=0.25 Kz=0.12	Kx=Ky=Kz=8.0E-04	Kx=Ky=0.25 Kz=0.12	8.5E-09 across, 8.5E-08 along	8.5E-09 (same as host rock)	No	5
Model 3	High-permeability shear zone	Kx=Ky=0.25 Kz=0.12	Kx=Ky=Kz=8.0E-04	Kx=Ky=0.25 Kz=0.12	8.5E-02 across, 8.5E-01 along	8.0E-03	No	5
NEW MODEL	Like Model 1, but high k middle Arbuckle	Kx=Ky=0.25 Kz=0.12	Kx=Ky=Kz=8.0E-03	Kx=Ky=0.25 Kz=0.12	8.5E-03 across, 8.5E-02 along	8.0E-04	No	5
NEW MODEL	Like Model 1, but very low k middle Arbuckle	Kx=Ky=0.25 Kz=0.12	Kx=Ky=Kz=8.0E-05	Kx=Ky=0.25 Kz=0.12	8.5E-03 across, 8.5E-02 along	8.0E-04	No	5
Model 4	Like Model 1 but reduced lower Arbuckle k	Kx=Ky=0.025 Kz=0.012	Kx=Ky=Kz=8.0E-04	Kx=Ky=0.25 Kz=0.12	8.5E-03 across, 8.5E-02 along	8.0E-04	No	5
Model 5	Like Model 1 but increased lower Arbuckle k	Kx=Ky=2.5 Kz=1.2	Kx=Ky=Kz=8.0E-04	Kx=Ky=0.25 Kz=0.12	8.5E-03 across, 8.5E-02 along	8.0E-04	No	5
Model 6	Like Model 1 but fault cuts Arbuckle	Kx=Ky=0.25 Kz=0.12	Kx=Ky=Kz=8.0E-04	Kx=Ky=0.25 Kz=0.12	8.5E-03 across, 8.5E-02 along	8.0E-04	Yes	5
NEW MODEL	Like Model 1 but reduced upper Arbuckle k	Kx=Ky=0.25 Kz=0.12	Kx=Ky=Kz=8.0E-04	Kx=Ky=0.025 Kz=0.012	8.5E-03 across, 8.5E-02 along	8.0E-04	No	5
NEW MODEL	Like Model 1 but increased upper Arbuckle k	Kx=Ky=0.25 Kz=0.12	Kx=Ky=Kz=8.0E-04	Kx=Ky=2.5 Kz=1.2	8.5E-03 across, 8.5E-02 along	8.0E-04	No	5
Model 1a	Like Model 1 but hypocenter at 3 km	Kx=Ky=0.25 Kz=0.12	Kx=Ky=Kz=8.0E-03	Kx=Ky=0.25 Kz=0.12	8.5E-03 across, 8.5E-02 along	8.0E-04	No	3
Model 1b	Like Model 1 but hypocenter at 7 km	Kx=Ky=0.25 Kz=0.12	Kx=Ky=Kz=8.0E-03	Kx=Ky=0.25 Kz=0.12	8.5E-03 across, 8.5E-02 along	8.0E-04	No	7
Model 3a	Like Model 3 but hypocenter at 3 km	Kx=Ky=0.25 Kz=0.12	Kx=Ky=Kz=8.0E-04	Kx=Ky=0.25 Kz=0.12	8.5E-02 across, 8.5E-01 along	8.0E-03	No	3
Model 3b	Like Model 3 but hypocenter at 7 km	Kx=Ky=0.25 Kz=0.12	Kx=Ky=Kz=8.0E-04	Kx=Ky=0.25 Kz=0.12	8.5E-02 across, 8.5E-01 along	8.0E-03	No	7

Table 2. Parameters for MODFLOW groundwater flow models completed during the grant period. Those labeled "new model" were completed after the grant period and are not discussed in detail.